Frost Heave due to Ice Lens Formation
in Freezing Soils
2. Field Application

D. Sheng, K. Axelsson and S. Knutsson

Department of Civil Engineering,
Luleå University of Technology, Sweden

An operational model for estimation of frost heave in field where stratified soil profile appears is presented. The model is developed from the research model described in part B. Soil layers are first classified into frost-susceptible layers (FSL) or non-frost-susceptible layers (NFSL). In an FSL, both heat flow and water flow are considered and ice lensing can occur. In a NFSL, only heat flow is possible and no ice lensing is allowed. The governing equations for heat and mass transfer are established for the time period when the frost front is moving within FSL. Capillarity and unsaturation are also considered. The operational model is verified by field measurements of heave amounts. Examples of application are given.

Introduction

As mentioned in part 1, very few existing frost heave models are satisfactory in all the following aspects

- Adequacy in describing the phenomenon,
- Validation by *e.g.* experimental data,
- Ease in determining input parameters, and
- Applicability in solving practical problems.

In an effort to overcome the shortcomings of existing models, we presented in Part 1 an alternative model for simulation of frost heave and ice lensing in saturated and

147

salt-free soil columns. In the model quasi-steady state heat and water flows were dealt with. Special attention was paid to the pore pressure and the permeability in the transmitted zone, *i.e.* the frozen fringe. The formation of each ice lens was simulated. The effect of overburden pressure was taken into account. The governing equations for heat balances were obtained in a similar manner as Gilpin (1980), but in different forms. The mass equations were newly presented. The criterion for ice lens initiation follows that by O'Neill and Miller (1985), *i.e.* that ice lens initiation takes place when and where the neutral stress approaches the total overburden pressure. The neutral stress was, however, calculated differently from O'Neill and Miller. The unfrozen water content in freezing soil was computed according to Kujala (1989). New expressions for the pore water pressure in the frozen fringe and for the variation of the permeability were presented. In comparison with the existing models such as by O'Neill and Miller (1985), the model we presented needs less input parameters but still covers the basic features of the phenomenon of frost heave. The model was also verified against laboratory data of heave and heaving rate for different soils and under different overburden pressures and different temperature gradients. It was found that the computed values are generally in a good agreement with the experimental data.

In this paper, the research model presented in Part 1 will be developed into an operational model which is expected to be capable of handling field conditions such as a stratified soil profile, unsaturated soils, capillarity and insulation. The operational model will be evaluated against field measurements of heave and frost depth at an insulated road section. The verified model will be applied to solve practical problems.

Operational Model

Soil Profile
Consider a soil profile consisting of different soil layers as shown in Fig. 1. We first classify the soil strata into frost-susceptible layers (FSL) and non-frost-susceptible layers (NFSL). In an FSL, water flow as well as heat flow is possible, ice lenses can form and frost heave may take place. Three thermal states can exist in an FSL, *i.e.* unfrozen, freezing (frozen fringe) and frozen states. The soil on the warm side of the frost front, where the temperature equals the freezing point, is unfrozen, between the latest ice lens and the frost front, freezing, on the cold side of the ice lens and including the lens, frozen. An FSL can be any moist soil saturated or unsaturated. In a NFSL, only heat flow occurs and ice lensing is not allowed. Therefore, no intermediate state, *i.e.* freezing, can exist. A NFSL can be any non-soil layer such as an insulation layer, or a layer of a very coarse soil such as gravel, or a layer of a dry soil. In Fig. 1, the first upper two and the lowest strata are classified as NFSL. The third stratum is an FSL.
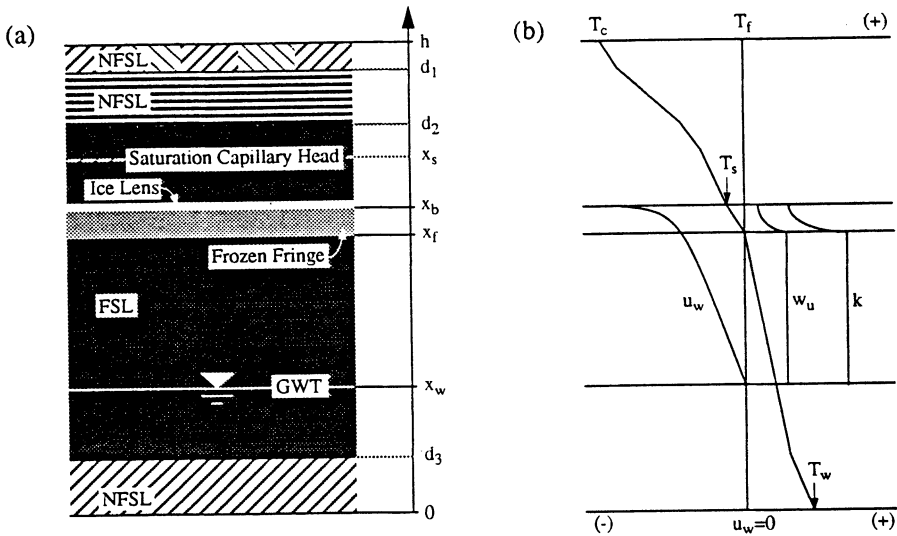
Fig. 1. Soil profile (a) and distributions of temperature and pore water pressure (b).

The coordinate origin is set to the warm boundary of the soil profile, with positive direction upward. The frost front is denoted by x_f and the warm surface of the latest ice lens by x_b. The groundwater table (GWT) is denoted by x_w, existing in the third layer. The saturation capillary head is denoted by x_s. The temperature at the ground surface is T_c, which is below the freezing point T_f. The temperature at $x=0$ is T_w, above the freezing point. The surface and bottom temperatures are either constant or vary as known functions of time.

The basic assumptions in the operational model follow those in the research model in Part 1:

- The temperature gradient in each layer is constant in space,
- The permeability of the frozen fringe decreases exponentially as a function of the temperature,
- The frozen fringe is always saturated by water or ice,
- The water flow in the frozen fringe and in the unfrozen soil reaches a steady state,
- The pore ice particles in the frozen fringe are connected to the latest ice lens as a rigid body,
- A new ice lens forms in the frozen fringe when and where the effective stress approaches zero.

The assumption that the frozen fringe is saturated by water and ice is in accordance with Miller (1980), who stated, with reference to the experiment by Dirksen and Miller (1966), that heave occurred only if the total moisture content just behind the frost front rose to about 90% pore saturation. In addition to the assumptions listed, the soil is assumed to be salt free.

149

Governing Equations

Since no ice lensing is allowed in a NFSL, it is of little interest to study the frost penetration within those layers. Therefore, attention is only paid to heat and mass flow when the frozen fringe (x_f, x_b) is located in the FSL. As in the research model in Part 1, it is assumed that the location (x_f, x_b) is known at the time level t_n. The aim is to determine the rate of heave during a small time step Dt and the new location of the frozen fringe at time level $t_{n+1}=t_n+\Delta t$. To do so, we first have to determine the segregational temperature T_s at x_b, the pore water pressure and the ice pressure at the time level t_{n+1}, and the rate of frost penetration and the rates of water flow in the frozen fringe and in the unfrozen soil during the time step Δt.

The governing equations for heat and mass flow can be obtained in a similar manner as in Part I. The heat balance at the warm surface of the latest ice lens x_b states

$$\bar{\lambda}_f \frac{T_s-T_c}{h-x_b} - \bar{\lambda}_{ff} \frac{T_f-T_s}{x_b-x_f} \equiv (1-I_b) V_i \rho_i L \qquad\qquad x = x_b \qquad (1)$$

where $\bar{\lambda}_f$ denotes the effective thermal conductivity of the current frozen zone, $\bar{\lambda}_{ff}$ the effective thermal conductivity of the current frozen fringe, h the total height of the soil profile at time t_n, L the specific latent heat of water, I_b the current volumetric ice content at x_b, ρ_i the density of ice, and V_i the rate of ice lensing or the rate of heave during the time step Δt.

The overall heat balance for the frozen fringe can be expressed as,

$$\bar{\lambda}_f \frac{T_s-T_c}{h-x_b} - \bar{\lambda}_u \frac{T_w-T_f}{x_f} = (V_i + \bar{I}(-\frac{dx_f}{dt})) \rho_i L \qquad x_w \leq x \leq x_v \qquad (2)$$

where dx_f/dt is the advancing rate of the frost front x_f or the frost penetration rate during Δt, $\bar{\lambda}_u$ the effective thermal conductivity of the current unfrozen zone, $\bar{I}$ the mean ice content in the current frozen fringe.

The mass conservation at x_b requires that the water flow to x_b equals the ice mass formed there

$$v_{ff} \rho_w = (1-I_b) V_i \rho_i \qquad\qquad x = x_b \qquad (3)$$

where v_{ff} denotes the water flow rate in the frozen fringe and ρ_w the density of bulk water.

The overall mass balance within the frozen fringe is slightly different from that in Part 1, because the unfrozen soil beyond the frozen fringe may not be saturated. The outflow of ice mass at x_b must balance the inflow of water mass at x_f plus the decrease of mass in the frozen fringe, *i.e.*

$$V_i \rho_i = v_u \rho_w + (S_r \rho_w - \rho_i) I (-\frac{dx_f}{dt}) \qquad\qquad x_f \leq x \leq x_b \qquad (4)$$

where S_r is the degree of saturation of the unfrozen soil at x_f.

In the case where the frost front is above the GWT, *i.e.* $x_f > x_w$, the rate of water flow in the unfrozen soil, v_u, can be determined by the Darcy law

$$v_u = -\frac{\bar{k}_u}{\rho_w g} \frac{u_w \, x_f}{x_f - x_w} + \rho_w g \qquad\qquad x_w \leq x \leq x_f \qquad (5)$$

where $\bar{k}_u$ is the effective permeability of the unfrozen soil between the frost front and the GWT, g the acceleration of gravity, and $u_w(x_f)$ the pore water pressure at the frost front x_f. Eq. (5) is assumed to be valid both for saturated and unsaturated flow. The pore water pressure in the frozen fringe is given as in Part 1

$$u_w(x) = L\rho_w \frac{T_s}{T_0} + \sigma \frac{\rho_w}{\rho_i} + (\nu_{ff}\rho_w g \, (\frac{e^{b(x_b - x_f)} - e^{b(x - x_f)}}{bk_u}) + \rho_w g(x_b - x) \quad (6)$$

where T_o is the freezing point of water, σ the total stress at the level x_b, k_{fu} the saturated permeability of the soil in the frozen fringe, and b a parameter which will be determined in a subsection. The generalized Clapeyron equation is included in Eq. (6).

The six Eqs. (1)-(6) form the basis of the frost heave model. Providing the location of the frozen fringe (x_f, x_b) and the material parameters are known, they can be solved by iteration for the six unknowns T_s, V_i, dx_f/dt, v_{ff}, v_u and $u_w(x)$.

If the frost front penetrates below the GWT, *i.e.* $x_f \leq x_w$, the pore water pressure at the frost front is then determined by

$$u_w(x_f) = (u_w - x_f)g\rho_w \qquad\qquad x = x_f \qquad (7)$$

In this case, the governing Eqs. (1), (2), (3) and (6) are still valid. Together with Eq. (7), the five equations are solved for the five unknowns T_s, V_i, dx_f/dt, v_{ff} and $u_w(x)$.

In the case where the frozen fringe is too thin for computation significance, the base of the latest ice lens is set to the frost front. The rate of water flow in the unfrozen zone is then in equilibrium with the rate of ice lensing and thus the frost front will remain stationary. The following equation is used instead of Eqs. (1) and (2)

$$\bar{\lambda}_f \frac{T_s - T_c}{h - x_b} - \bar{\lambda}_u \frac{T_w - T_s}{x_b} = V_i \rho_i L \qquad (8)$$

The mass equation is simplified to

$$V_i \rho_i = \nu_u \rho_w \qquad (9)$$

Eqs. (5)-(6) are still valid. Together with Eqs. (8) and (9), the four equations can be solved for the four unknowns T_s, V_i, $u(x_f)$ and v_u.

Location of the Frozen Fringe

So far the governing equations have been established by assuming that the location

of the frozen fringe is known. Now let us discuss how to locate the frozen fringe at each time step.

If the frozen fringe (x_f, x_b) is known at the time level t_n, the frost penetration rate dx_f/dt can be determined and the new position of the frost front at the time level $t_{n+1}=t_n+\Delta t$ is $x_f+(dx_f/dt)\Delta t$. The position of the warm surface of the latest ice lens x_b will remain fixed unless a new ice lens appears within the frozen fringe. A new ice lens will form when and where the effective stress vanishes. The effective stress can be computed approximately as

$$\sigma' = \sigma - \frac{(n-I)}{n}u_w = \frac{I}{n}u_i = \sigma - u_n \qquad\qquad x_f \leq x \leq x_b \qquad (10)$$

where σ' denotes the effective stress, u_n the effective pore pressure or the neutral stress, n the soil porosity and I the ice content.

The ice pressure u_i in Eq. (10) can be determined by the generalized Clapeyron equation

$$\frac{u_w}{\rho_w} - \frac{u_i}{\rho_i} = L \frac{T}{T_0} \qquad\qquad (11)$$

The neutral stress u_n can then be expressed by

$$u_n = (1 - \frac{I}{n} + \frac{I}{n}\frac{\rho_i}{\rho_w})u_w - \frac{I}{n}\frac{L\rho_i}{T} T \qquad\qquad x_f \leq x \leq x_b \qquad (12)$$

Eq. (12) is non-linear in temperature because of the temperature-dependence of the ice content I. The derivative $\delta u_n/\delta x$ is a very complex function of x and it is not easy to solve the condition $\delta u_n/\delta x=0$ for the position x_{nb}, where the maximum neutral stress takes place. Therefore, the frozen fringe (x_f, x_b) is divided into many equal intervals and the neutral stress u_n is computed at each dividing point. The maximum neutral stress and its position can be determined by interpolation. This maximum value is then compared with the total stress. If the total stress is exceeded, a new ice lens is expected to form. The new frozen fringe at the time level t_{n+1} is (x_{bn}, x_f).

To locate the starting position of the frozen fringe, the method by trial and error is used. Since there is no need to study the frost penetration within any NFSL, the first position of the cold boundary of the frozen fringe x_b can reasonably be set to the upper boundary of the first FSL. By assuming a trial temperature T_b at x_b, the position of the frost front x_f can be found by interpolation of the temperature field from $x=0$ to $x=x_b$. The governing equations can then be solved for the segregational temperature T_s'. The procedure is repeated until T_s approximately equals T_b.

Material Parameters

The governing equations contain a number of material parameters that have to be determined. Such parameters include the effective thermal conductivity and the permeability of a multi-layer structure, the thermal conductivity and the permeabil-

ity of a multi-phase layer, and the ice content of the frozen fringe.

The effective value of a conductive parameter of a stratified profile *e.g.* the effective thermal conductivity and the effective permeability, can be represented by the harmoic mean

$$\bar{\Lambda} = L / (\frac{l_1}{\Lambda_1} + \frac{l_2}{\Lambda_2} + \dots) \tag{13}$$

where $\bar{\Lambda}$ denotes the effective value to be determined, L the total thickness, l_n the thickness of the nth layer, and Λ_n the parameter of the nth layer.

The thermal conductivity of a soil saturated by water or ice can be expressed by the geometric mean

$$\lambda_{sat} = \lambda_s^{1-n} \lambda_w^{n-\bar{I}} \lambda_i^{\bar{I}} \tag{14}$$

where the subscripts s, w and i respectively stands for soil solid phase, water phase and ice phase.

The thermal conductivity of an unsaturated soil is given by Johansen (1975)

$$\lambda \equiv (\lambda_{sat} - \lambda_{dry}) K_e + \lambda_{dry} \tag{15}$$

where λ_{dry} is the thermal conductivity of the dry soil and K_e a parameter called the Kersten number.

The permeability of a partially frozen soil is a function of the temperature and the soil, Horiguchi and Miller (1983). A representative relationship between permeability and temperature is unfortunately not available yet. Therefore a test function, which was used in Part 1 and which demonstrated good performance, is here again applied temporarily. This function states that the permeability of the frozen fringe decreases as an exponential function of the temperature

$$k_{ff} = k_{fu} e^{c(T-T_f)} = k_{fu} e^{-b(x-x_f)} \qquad\qquad x_f \le x \le x_b \tag{16}$$

The parameter c or b in Eq. (16) can either be treated as an input parameter or, as a first approximation, be estimated as follows. If it is assumed that

$$k_{ff} = k_{fu} \left(\frac{W_u(x_b)}{n} \right)^9 = k_{fu} \left(\frac{n-I_b}{n} \right)^9 \tag{17}$$

as done by O'Neill and Miller (1985), the parameter b can be determined by substituting Eq. (17) into Eq. (16). Eq. (16) can be replaced or modified in future if more information on the subject comes up.

The permeability k_{ps} of a partially saturated soil in the unfrozen state, can either be treated as an input parameter or approximated by a given saturated permeability, Hillel (1971)

$$k_{ps} \equiv k_s \, S_r^m \tag{18}$$

where k_s is the saturated permeability and m a soil parameter that should be given.

The volumetric ice content in the frozen fringe equals $(n\text{-}W_u)$, with W_u denoting the volumetric unfrozen water content. The unfrozen water content is a function of the temperature or a function of the pressure difference $(u\text{-}u_i)$. The function given by Kujala (1989) was used in Part 1 and is applied again here

$$n - I = W_u(T) = W_0 \, e^{\alpha(T)^\beta} \tag{19}$$

where W_O is the initial volumetric water content, α and β constants depending on the specific surface area and pore geometry of the soil. The constant β approximately equals 2 for most of soils of interest. The constant α can be determined by substituting into Eq. (20) an unfrozen water content at a subfreezing temperature *e.g.* -1.0 °C.

Computational Strategies

The model presented in the previous text has been implemented on a personal computer. The computation scheme is described as follows. At each time step, the material parameters are first computed, based on the current frozen fringe and the segregational temperature. Thereafter, the governing equations are solved for the rate of ice lensing (heaving) V_i, the rate of frost penetration dx_f/dt, the distribution of pore water pressure within the frozen fringe $u_w(x)$, and the new segregational temperature T_s. Finally we determine if there is any new ice lens initialized in the frozen fringe, in which case the length of the soil profile and the position of frozen fringe are modified accordingly. The procedure is then repeated for next time step.

The computer program was written in *Turbo C* and computer graphics was used to represent the heaved soil columns enclosing ice lenses, history diagrams of the heave, frost front, segregational temperature and suction in the pore water pressure in the frozen fringe. The input parameters include boundary temperatures, GWT, dry density, water content, degree of saturation, thermal conductivity, permeability and a unfrozen water content at a subfreezing temperature. The time step for computation, another input parameter, should be given such a small value that the frost penetration during any single time step does not exceed the half thickness of the FSL that contains the frozen fringe.

Field Verification

In this section the operation model presented in the previous section is evaluated by the field data measured at a test road located at Piteå, 900 km north of Stockholm. Heave and ground temperature were measured at the centre and the shoulders of the road, Fig. 2, at a time interval of approximately 4 weeks through the winter 1985/86.
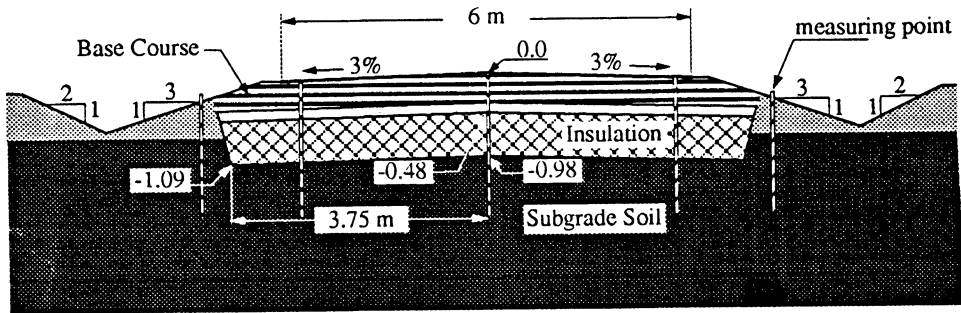
Fig. 2. Road section with insulation of 50 cm thick.

The test road was originally constructed to study the efficiency of expanded clay balls as an insulation layer for frost protection. A layer of expanded clay balls of a thickness varying from 0 to 50 cm was placed under the subbase course, the gravel, Fig. 2. At one site, a layer of sand of a thickness of 85 cm was used instead of the insulation, Fig. 3a. The subgrade soil is a highly frost-susceptible clayey silt of several metres, occasionally enclosing gravel pockets, Fig. 3b.

In the simulation, the mean air temperature is used as the boundary condition at the ground surface. The ground temperature is assumed to be 3°C and remains constant at the depth of 3.5 m. The simulation is initiated at the time when the measured frost penetration reaches the subgrade soil and stopped at the end of March 1986. The groundwater table during the freezing period is assumed to remain at the depth of 1.5 m. The silt above the GWT is assumed to be saturated by capillarity. The dry density, the water content and the thermal conductivity of the silt were measured in laboratory using undisturbed samples. The permeability used in the computation is an average value of the soil at temperatures close to 0°C. The unfrozen water content at -1°C is 7% by dry weight, back-estimated from one measured heave at the section shown by Fig. 3a. The material properties are listed in Table. 1.

Table 1 – Material properties

Material	Surface & Base Course (NFSL)	Gravel (NFSL)	Sand (NFSL)	Silt (FSL)	Insulation (NFSL)
Dry density, kg/m3	2100	2200	1900	1600	340
Water content,%	5	3	10	25	25
Degree of saturation,%			80	100	10
Permeability, cm/s				10_{-7}	
Thermal conductivity	1.5	2.0	1.4	1.1	0.10
Thickness, cm	16~34	10~14	85	~250	0~50
Unfrozen water content at -1.0°C,%				7†	

† Back estimated from the point marked in Fig. 4a.

a) 50 cm sand   b) 15 cm Insul.   c) 30 cm Insul.   d) 50 cm Insul.

Surface and base course   Gravel   Sand
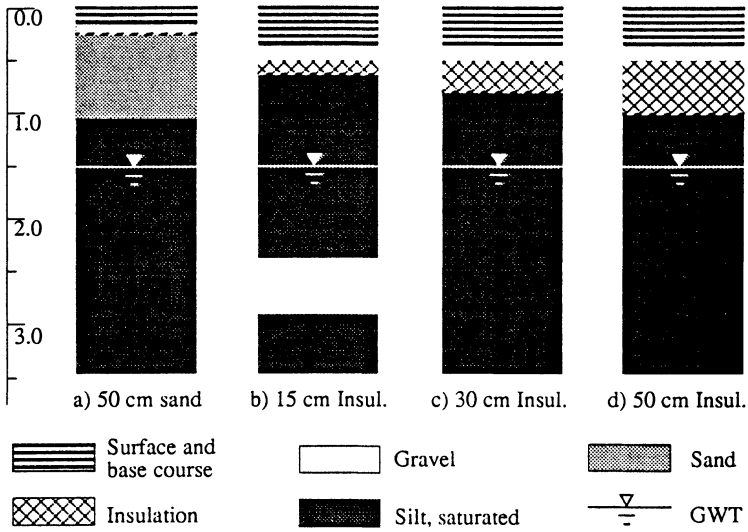
Insulation   Silt, saturated   GWT

Fig. 3. Material profiles under the road centre, with varying insulation thicknesses.
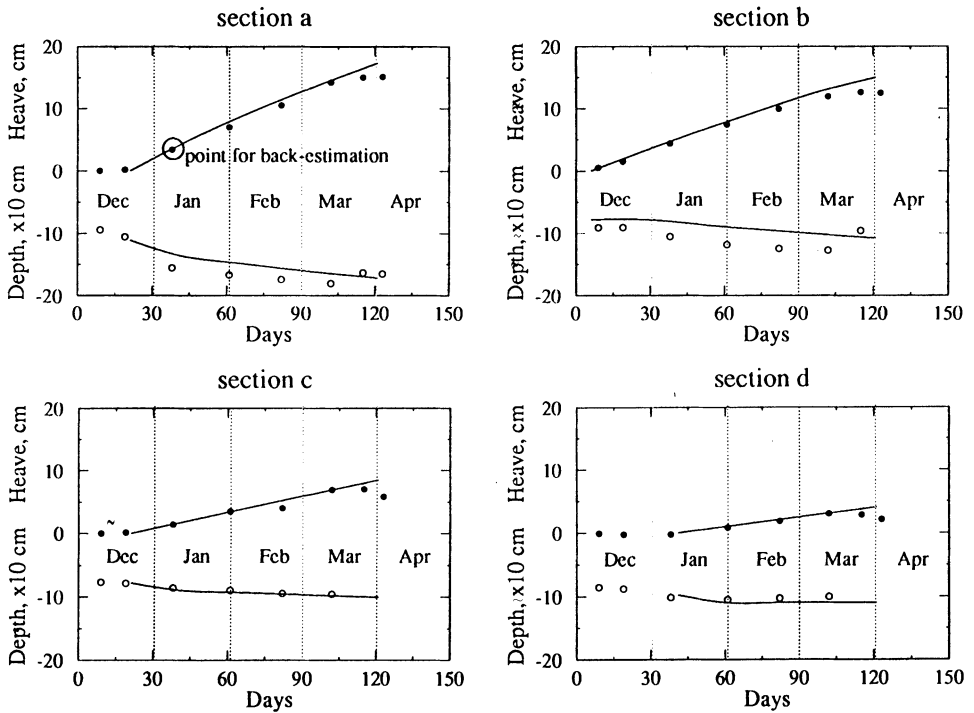
Fig. 4. Computed and measured frost heave and frost depth (points: measured, lines: computed).

156

Table 2 – Boundary conditions

Section	T_c, °C	Freezing Period	Freezing Index, °C day
a) no insulation	-10	Dec 21, 1985 – Mar 31, 1986	1000
b) 15 cm insulation	-11	Dec 1, 1985 – Mar 31, 1986	1265
c) 30 cm insulation	-10	Dec 21, 1985 – Mar 31, 1986	1000
d) 50 cm insulation	- 9	Jan 10, 1986 – Mar 31, 1986	720

The computed values of frost depth are, however, not in a good agreement with the measured ones. For sections a and b, an underestimation of up to 25% is observed. This underestimation occurs very early. The reason may again be attributed to the lower surface temperature used in the simulation than the actual values of December and January, which was close to -21°C in average. The actual frost penetration stopped in January, due to the rising of the surface temperature. This 'step freezing' effect is, however, smoothbored in the simulation by the use of an average temperature. For sections c and d, the thick insulation layers themselves also smoothed the variation in the surface temperature and thus better agreements are obtained.

Application Examples

Efficiency of Insulating Materials in Reducing Frost Heave

In road construction in cold regions, it is very common to place a layer of insulation or non-frost-susceptible material within the subbase course, in order to reduce frost penetration and heave. Various materials *e.g.* extruded and expanded polystyrene, expanded clay balls, wet bark, compressed peat and gravel have been used for this purpose. In this section the effectiveness of the materials commonly used in practice are evaluated by the operational model presented.

For convenience we use the same road section shown in Fig. 3c and the same subgrade soil, *i.e.* the silt listed Table 1, but with varying thicknesses of insulating or non-frost-susceptible materials. The temperature at the ground surface varies between -5 to -15°C and the temperature at the depth of 4 m remains 3°C. The initial position of the frost front is set to the upper boundary of the subgrade soil. The heave amounts after freezing of 100 days are computed for various thicknesses of insulation. The difference between the heave amounts without and with insulation, in percentage of the heave without insulation, is plotted versus the thickness of the insulation for three design values of freezing index in Fig. 5. It can be noted that the most effective insulation materials are the synthetic insulation (*e.g.* extruded polystyrene) and the expanded clay balls. The wet bark and the compressed peat cause approximately the same amount of reduction in the heave. It is found by test computations that the influences of the properties of the subgrade soil on the curves in Fig. 5 are insignificant, as along as the reduced heave is plotted in percentage of the
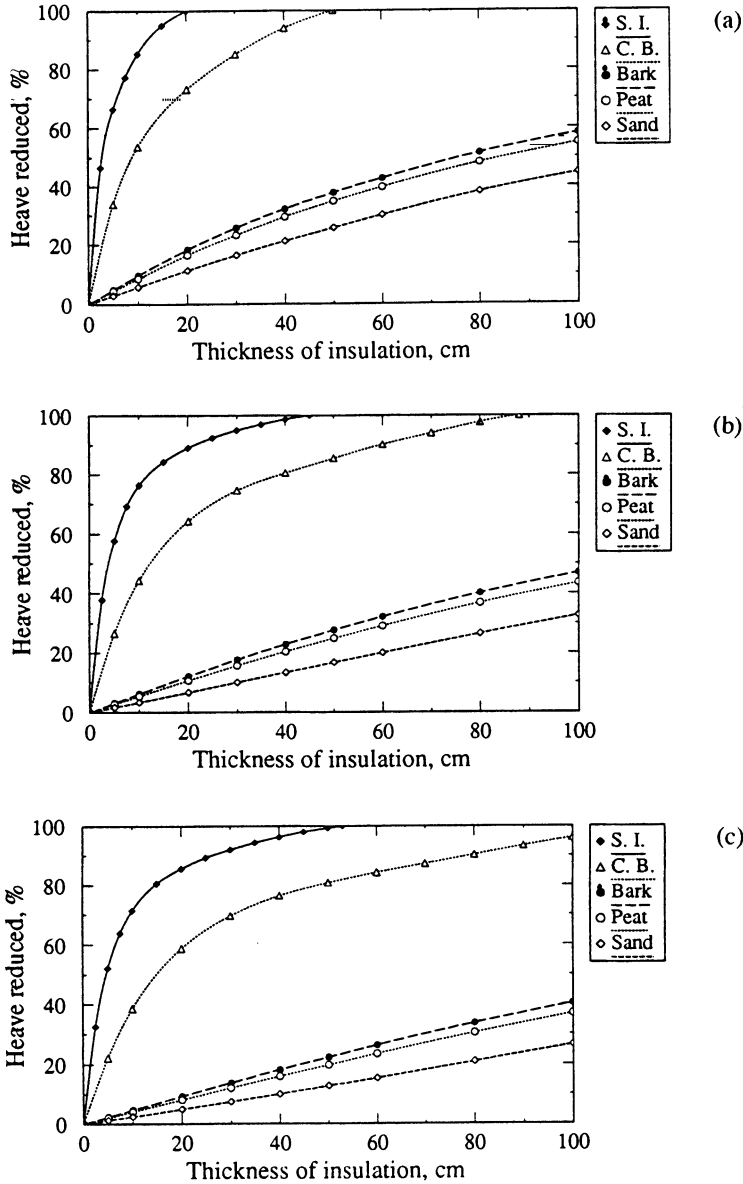
Fig. 5. Heave reduced *versus* the thickness of insulation for different design freezing indices.
Heave reduced equals the difference between the heave without and with insulation,
in percentage of the heave without insulation.
(a) Design Freezing Index = 500°C×days
(b) Design Freezing Index = 1000°C×days
(c) Design Freezing Index = 1500°C×days

158

Table 3 – Properties of replacement materials

Replacement	Dry Density kg/m³	Water Content % by weight	Thermal Conductivity W/m°C
Synthetic Insulation (S. I.)ø	40	25	0.04
Expanded Clay Balls (C. B.)	340	25	0.1
Bark	350	186	0.45
Compressed Peat	400	120	0.6
Sand, Gravel	2000	5	2

† Average values of polystyrene, Nordal and Refsdal (1989).

heave without insulation. Therefore, the curves shown in Fig. 5 can also be used, independently of soil profile and soil properties, to evaluate the effectiveness of the insulating materials in reducing heave.

In Fig. 6, the design thickness of the insulation is plotted *versus* the freezing index for different design values of heave. It is observed that the design thickness of the insulation increases almost linearly as the freezing index increases. The slopes of the lines in Fig. 6 are, however, dependent on the soil profile and soil properties used. Therefore, this diagram can not be applied for other soil profiles different from that shown by Fig. 3c.

It should be noted that the freezing indices indicated in Figs. 5 and 6 do not count the time when the frost front is penetrating within the surface and base courses and the insulation layer. As the thickness of the insulation layer increases, the actual freezing time of the subgrade soil decreases. Therefore, when the diagram Fig. 6 is used to estimate the efficiency of insulation, the freezing period before the frost front reaches the upper boundary of the subgrade soil has to be subtracted from the total freezing time. This freezing period can be estimated by *e.g.* the Neumann solution.
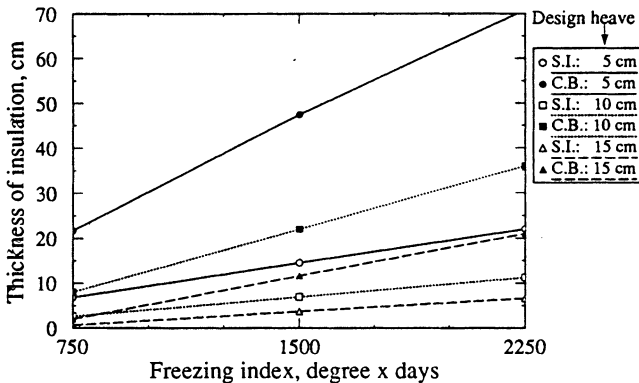

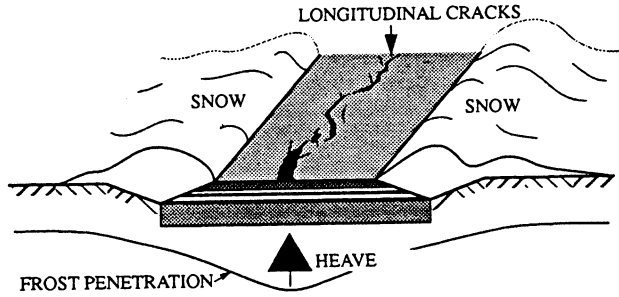Fig. 6. Thickness of insulation *versus* freezing index for different design values of heave.

Fig. 7. Longitudinal cracks caused by differential heave due to snow insulation.

Effect of Snow Cover on Differential Frost Heave

Non-uniform frost penetration used to cause differential heave. That is often the case when a road is covered by snow at the shoulders so that a deeper frost penetration and hence a larger heave takes place at the centre of the road. The resulting damage on asphalt pavements is characterized by the occurrence of longitudinal cracks at the centre of the road, Fig. 7. This problem can approximately be studied by the operational model described above.

Consider the road section shown in Fig. 3a.The shoulders of the road are covered by snow, Fig. 7. The horizontal heat flow in the ground is assumed to be zero so that the actual three-dimensional or at least two-dimensional problem can be simulated by the one-dimensional model. As a first approximation, the material profile at the shoulders of the road is assumed to be the same as at the centre of the road, but with an additional layer of snow on the top. The snow may be in a loose, medium or dense state, with a density of 300, 400 and 500 kg/m^3 and a thermal conductivity 0.25, 0.46 and 0.71 W/mK respectively. The initial position of the frost front is set to the upper boundary of the FS subgrade soil, regardless of the snow cover. The relative heave, *i.e.* the ratio between the heave at the shoulders to that at the centre is computed and plotted as a function of the thickness of the snow cover, Fig. 8.

For the medium snow, the heave is computed for three surface temperatures. It is of interest to note that the variation in the relative heave due to the change in surface temperature is relatively small. Therefore, the diagram can be applied, independently of the surface temperature, to predict the heave reduced due to snow insulation. It should be pointed out that the actual value of the relative heave is underestimated by Fig.8 as the thickness of snow increases, because the freezing time before the frost front reaches the subgrade soil is not considered. This time period increases as the thickness of snow increases. For a snow layer of the thickness of 1 m, no heave could take place if the boundary temperature is higher than -5°C. Nevertheless, the diagram Fig. 8 gives us the possibility to have a quick estimation of the differential heave caused by the snow covers on road shoulders.
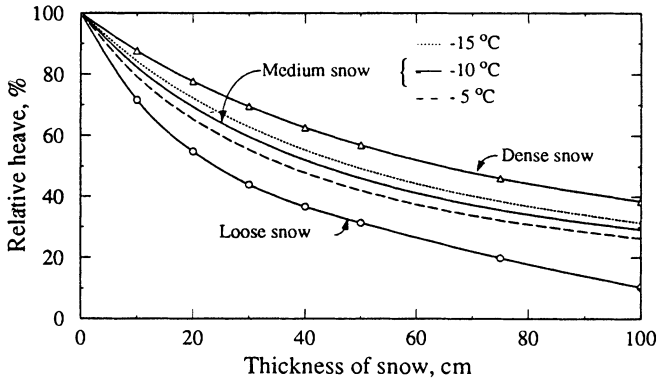
Fig. 8. Relative heave *versus* thickness of snow cover. Relative heave = (heave with snow)/ (heave without snow).

Effects of GWT and Saturation on Frost Heave

The groundwater table (GWT) provides the source of mass needed by ice segregation and is one of the important parameters that influence frost heave. The pioneer investigation of frost heave by Beskow (1935) already showed that lowering the GWT leads to a smaller rate of heaving. The experimental studies by Kinosita (1979) also demonstrated that the higher the initial water level was, the larger the heave amount would be. In construction practising in cold regions, water-tight membranes are used to shut off ground water inflow from frost active zone, in order to reduce heave amount, Kinosita (1989). In this section the effect of GWT on frost heave is studied by the model presented.

The site of the example problem is located outside the town of Jokkmokk, 170 km northwest from Luleå. Damage of an uninsulated house has been observed and the distortion is suspected to be related to the rising of the GWT, from the depth of 4.3 m to 3.3 m, due to the rising of the water level in a neighbouring water reservoir. The damages have been observed since the second spring after the rising of the GWT, Mattsson (1993). The soil profile under the displaced house is shown by Fig. 9. Outside the house, the average thickness of the snow cover on the ground surface during winter period, which is about 180 days at Jokkmokk, is 50 cm. The mean cold temperature during the period is -13°C. The ground temperature remains approximately constant at 5°C at 5 m deep. It is assumed that the ground surface is flat so that the one-dimensional model can be used to calculate the heave amount and frost depth outside the house, both before and after the rising of the GWT.

The underlying soil is a sandy silt and its main properties are determined by laboratory tests as follows: passing 0.063 mm (silt) 51.2%, passing 0.002 mm (clay) 0.9%, dry density ρ_d=2,000 kg/m^3, saturated water content w=14% by dry weight, saturated permeability at +0°C k_s=1.43×10^{-5} cm/s, and total capillary head of 300 cm. In
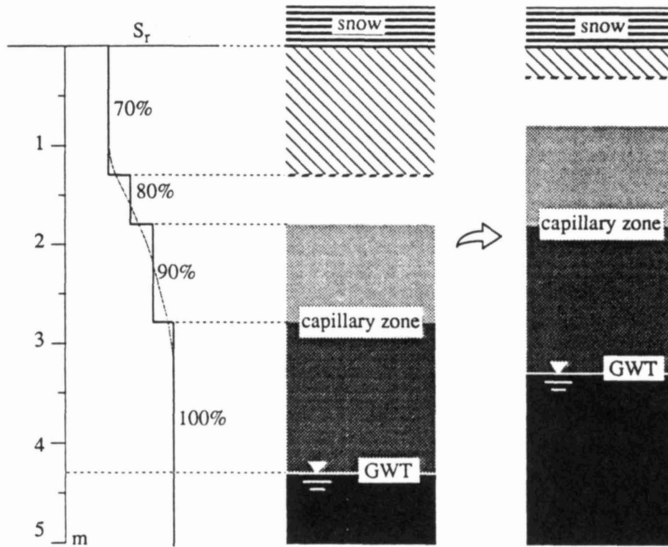
Fig. 9. Soil profile and variation in the saturation degree.

addition, it is assumed that the unfrozen water content at -1°C is 3% by dry weight and the thermal conductivity of the soil solid is 3 W/mK. The total capillary head is assumed to consist of 150 cm saturated, 100 cm with 90% saturation and 50 cm with 80% saturation. The degree of saturation above the capillary zone S_r equals 70%. The capillary head varies in accordance with the changes in the GWT. The permeability of the unsaturated soil is determined as follows, Kézdi (1979)

$$k_{ps} = k_s \left(\frac{S_r - S_0}{1 - S_0} \right)^3 \tag{20}$$

where S_o is the upper threshold of the degree of saturation and here is assumed to be 50% for the sandy silt.

The computed values of heave and frost depth are plotted *versus* the depth of the GWT in Fig. 10. It can be noted that as the GWT rises, the heave amount increases but the depth of frost penetration decreases. The predicted heave increases from 1.0 to 4.2 cm, *i.e.* 420%, when the GWT is raised from 4.3 to 3.3 m deep. This amount increase in the heave might be the cause of the damage observed. However, a more decisive conclusion should be made based on the analysis of the thaw settlement, particularly the non-uniform thaw settlement caused by *e.g.* the sun effect.

The results shown in Fig. 10 is qualitatively in agreement with the experimental observations by Kinosita (1979). We can also explain the influence of the GWT as follows. In the first place, a rise in the GWT will cause a rise in the capillary head too. The rise in the capillary head may increase the saturation degree of the soil above the GWT. As a result, the permeability of the soil may also be increased. In Part 2 we
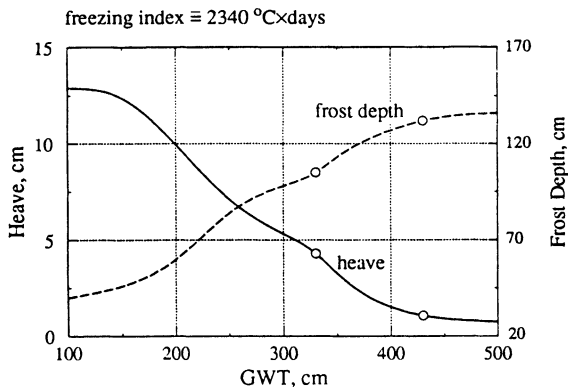
162

freezing index ≡ 2340 °C×days

Fig. 10. Computed values of heave and frost depth *versus* the groundwater table.
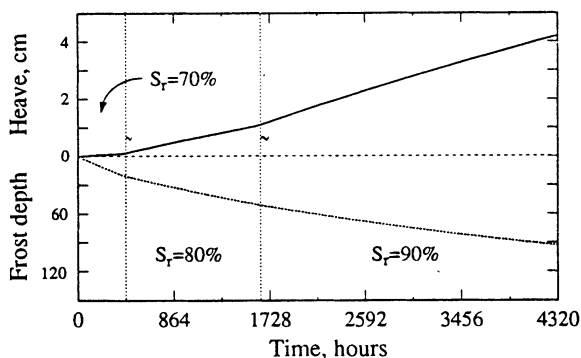

Fig. 11. Heave and frost depth *versus* time, GWT= 3.5 m.

have already shown that the permeability is a sensitive parameter to frost heave. As the permeability increases, the rate of water flow and hence the rates of ice lensing and heaving increase. Therefore, the total heave is expected to increase. In the second place, the rise in the GWT will also reduce the distance between the GWT and the frost front at the early stage of freezing. In consequences the hydraulic gradient, the rate of water flow and the rates of ice lensing and heaving are again expected to increase. However, the increased rate of water flow will lead to a larger amount of latent heat transferred to the frozen fringe. Also the increased saturation degree means more latent heat available *in situ*. Therefore, the rate of frost penetration is expected to decrease as the GWT rises.

It is of interest to study the history diagram of the computed heave and frost depth. From Fig. 11, we note that there exist three different heaving rates during the entire freezing period. These three rates respectively correspond to three different degrees of saturation. When the frost front initially penetrates in the unsaturated
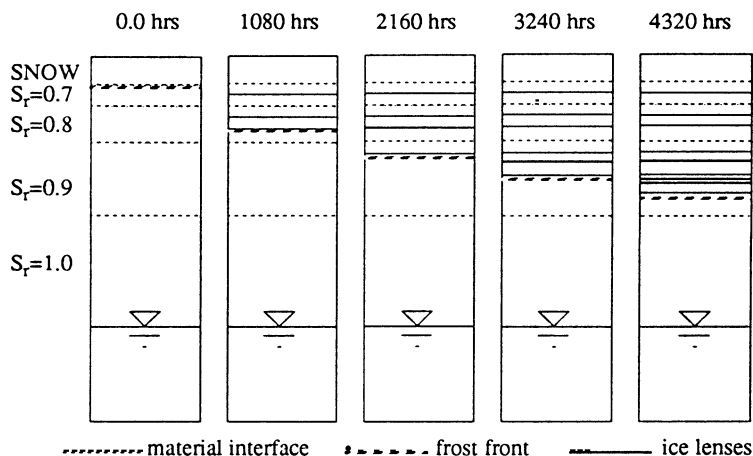
163

Fig. 12. Heaved soil columns with ice lenses enclosed, GWT=3.5 m.

zone where S_r=70%, few ice lenses can form (Fig. 12) and the corresponding rate of heaving is the lowest. At the time equal to 480 hours the frost front reaches the capillary zone where S_r=90%, and more ice lenses can form and the heaving rate increases accordingly. The heaving rate reaches its maximum when the frost front penetrates into the saturated zone. This saturation-dependent ice lens formation implies that the discretization of the soil profile above the GWT will have some influence on the simulated ice lens distribution. However, it has been found during trial computation that the total heave is not much influenced by the discretization.

The effect of unsaturation on the frost depth is not very obvious in Fig. 11. As the frost front moves from the unsaturated soil to the saturated soil, the rate of frost penetration experiences a slight decrease.

Summary and Conclusion

In this paper an operational model for calculation of frost heave in field where stratified soil profiles and unsaturation may occur has been presented. The model has been developed from the research model presented in Part 1. Soil layers have been classified into frost-susceptible layers (FSL) or non-frost-susceptible layers (NFSL). In an FSL, both heat flow and water flow have been considered and ice lensing can occur. In a NFSL, only heat flow has been allowed to take place and ice lensing can not occur. The heat balance equations have been obtained for the entire domain of interest, whereas the water flow equations have been established only for the layers of the type FSL.

The model has been implemented on an personal computer. The input parameters

164

to the computer program include the total density and the thermal conductivity of each NFSL, the dry density, the initial water content, the permeability, the degree of saturation, the thermal conductivity, the unfrozen water content at a subfreezing temperature of each FSL, the boundary temperatures and the depths of the groundwater table. The output of the computer program are heaved soil columns with ice lenses, history diagrams of heave, frost depth, segregational temperature and suction in pore water pressure in the frozen fringe.

The model was evaluated against field data. The computed values of heave are in good agreement with the measured data. Discrepancies between the predicted and the measured values of frost depth have been observed when the actual varying temperature at the road surface was approximated by a mean temperature of the entire freezing period.

The applicability of the model to solving practical problems has been demonstrated through example problems. The effectiveness of the commonly-used insulating materials in reducing frost heave has been evaluated. The differential frost heave caused by the snow cover on road shoulders has been estimated, as a function of the snow thickness. The effect of the ground water table on frost heave has also been studied. The results obtained are generally reasonable.

Through the results and discussion presented in the previous paper and in this paper, it has been demonstrated that the complex phenomenon of frost heave indeed can be simulated in a relatively simple way. Factors that have to be taken into account in simulation of frost heave are heat flow, water flow and ice lens formation. Major parameters influencing frost heave include boundary temperatures, thermal conductivity of the soil, hydraulic conductivity of the soil, unfrozen water content at subfreezing temperature of the soil and overburden pressure. The most difficult part in simulation of frost heave lies on the determination of material parameters such as permeability of an unsaturated soil and of a freezing soil. For future research, the following areas are expected to be highlighted

- The correlation between the unfrozen water content of a frozen soil and the soil characteristics should be further studied experimentally. In future, the unfrozen water content at a subfreezing temperature, which is a very sensitive parameter in the frost heave model but can not be easily determined in practice, may be calculated, based on reliable expressions, from *e.g.* the specific surface area and/or clay content of the soil.
- In reality, boundary conditions and soil parameters are often stochastic, both in time and in space. The deterministic model should be modified to be able to account for the stochastic behaviour of parameters.
- In the case where the gradients in temperature and in water pressure are significantly non-linear and multi-dimensional problems are involved, more advanced methods have to be used to solve a complete frost heave model such as the rigid ice model by O'Neill and Miller (1985).

Notations

FSL	Frost-Susceptible Layer	
NFSL	Non-Frost-Susceptible Layer	
g	Acceleration of gravity	m/s^2
h	Length of soil column	m
I	Ice content	
I_b	Ice content at the base of the growing ice lens	
$\bar{I}$	Mean ice content in the frozen fringe	
k	Permeability	m/s
k_{ff}	Permeability of the frozen fringe	m/s
k_{fu}	Saturated permeability of the soil in the frozen fringe	m/s
k_{ps}	Permeability of partially saturated soil	m/s
k_s	Saturated permeability	m/s
$\bar{k}_u$	Effective permeability of unfrozen zone	m/s
L	Specific latent heat of water	J/kg
n	Porosity of soil	
q	Overburden pressure	Pa
S_r	Degree of saturation	%
t	Time	s
Δt	Time step	s
T	Temperature	°C
T_c	Applied temperature at the cold side	°C
T_f	Freezing temperature soil moisture	°C
T_o	Freezing point of bulk water	degree Kelvin
T_s	Segregational temperature	°C
T_w	Applied temperature at the warm side	°C
u_i	Ice pressure	Pa
u_n	Neutral stress	Pa
u_w	Pore water pressure	Pa
v_{ff}	Rate of water flow in the frozen fringe	m/s
v_u	Rate of water flow in the unfrozen soil	m/s
V_i	Rate of ice lensing (rate of heave)	m/s
W_o	Initial water content by volume	
x_b	Base position of the growing ice lens	m
x_f	Position of frost front (0-isotherm)	m
x_{nb}	Base position of the new ice lens	m
$\bar{\lambda}_f$	Effective thermal conductivity of frozen zone	W/(m°C)
λ_{ff}	Thermal conductivity of frozen fringe	W/(m°C)
λ_i	Thermal conductivity of ice	W/(m°C)
λ_s	Thermal conductivity of soil solid	W/(m°C)
$\bar{\lambda}_u$	Effective thermal conductivity of unfrozen zone	W/(m°C)
λ_w	Thermal conductivity of water	W/(m°C)
ρ_i	Density of ice	kg/m^3
ρ_w	Density of water	kg/m^3
σ'	Effective stress	Pa

Acknowledgement

References

Anderson, D. M., and Tice, A. R. (1973) The unfrozen interfacial phase in frozen soil-water systems, *Ecological Studies*, Springer Verlag, *Vol. 4*, pp. 107-124.

Beskow, G. (1935) Soil freezing and frost heaving with special application to roads and railroads, *Swedish Geology Survey Yearbook, Vol. 26(3)*, Ser. C, No. 375, Translated by J. O. Osterberg, Tech. Inst., Northwestern University, Evanston.

Burt, T. P., and Williams, P. J. (1976) Hydraulic conductivity in frozen soils, *Earth Surface Processes, Vol. 1*, pp. 349-360.

Farouki, O. T. (1986) *Thermal properties of soils*, Clausthal-Zellerfeld, Trans Tech Publication.

Gilpin, R. R. (1980) A model for the prediction of ice lensing and frost heave in soils, *Water Resour. Res., Vol. 16, No. 5*, pp. 918-930.

Harlan, R. L. (1973) Analysis of coupled heat and mass transfer in partial frozen soil, *Water Resour. Res., Vol. 9, No. 5*, pp. 1314-1323.

Hillel, D. (1971) *Soil and water – physical principles and processes*, Academic Press, New York.

Holden, J. T., Piper, D., and Jones, R. H. (1985) Some development of a rigid-ice model of frost heave, Proc. 4th Int. Symp. Ground Freezing, (S. Kinosita and M. Fukuda, eds.) 5-7 August, 1985, Sapporo, Japan, Elsevier, pp. 93-98.

Hopke, S. (1980) A Model for frost heave including overburden, *Cold Reg. Sci. Tech., Vol. 3*, pp.111-127.

Horiguchi, K., and Miller, R. D. (1983) Hydraulic conductivity functions of frozen materials, Proc. 4th Int. Conf. Permafrost, Fairbanks, Alaska, pp. 504-508.

Johansen, O. (1975), Thermal conductivity of soils, Ph.D. Thesis, Trondheim, Norway.

Kézdi, A. (1979) *Soil physics – selected topics*, Elsevier, Budapest.

Kinosita, S. (1979) Effects of initial soil-water conditions on frost heaving characteristics, Ground Freezing, Proc. 1st Int. Symp., Bochum, March 8-10, 1978, Elsevier, pp. 41-52.

Kinosita, S. (1989) Preventing measures against frost action in soils, Frost in Geotechnical Engineering, Int. Symp., Saariselkä, Finland, March 13-15, 1989, Technical Research Centre of Finland, Vol. 2, pp. 733-748.

Konrad, J. M., and Morgenstern, N. R. (1980) A mechanistic theory of ice lens formation in fine-grained foils, *Can. Geotech. J., Vol. 17*, pp. 473-486.

Konrad, J. M., and Morgenstern, N. R. (1981) Segregational potential of freezing soil, *Can. Geotech. J., Vol. 18*, pp. 482-491.

Kujala, K. (1989) Unfrozen water content of finish soils measured by NMR, Frost in Geotechnical Engineering, Int. Symp. at Saariselkä, Finland, March 13-15, 1989, Technical Research Centre of Finland, Vol. 1, pp. 301-310.

Mattsson, H. (1993) Personal communication, Luleå University of Technology, Sweden.

Miller, R. D. (1980) Freezing phenomena in soils, in *Applications of Soil Physics* (D. Hillel, ed.), Academic Press, pp. 254-299.

Nixon, J. F. (1991) Discrete ice lens theory for frost heave in soils, *Can. Geotech. J., Vol. 28*, pp. 843-859.

Nordal, R. S., and Refsdal, G. (1989) Frost protection in design and construction, Frost in Geotechnical Engineering, Int. Symp., Saariselkä, Finland, March 13-15, 1989, Technical Research Centre of Finland, Vol. 1, pp. 127-163.

O'Neill, K., and Miller, R. D. (1985) Exploration of a rigid -ice model of frost heave, *Water Resour. Res., Vol. 21, No. 3*, pp. 281-296.

Padilla, F., and Villeneuve, J. P.(1992) Modeling and experimental studies of frost heave including solute effects, *Cold Reg. Sci. Tech., Vol. 20*, pp. 183-194.

Penner, E. (1986) Aspects of ice lens growth in soils, *Cold Reg. Sci. Tech., Vol. 13*, pp. 91-100.

Saarelainen, S. (1992) Modelling of frost heaving and frost penetration in soils at some observation sites in Finland, the SSR model, Technical Research Centre of Finland, Espoo, Finland.

Shen, M., and Ladanyi, B. (1987) Modelling of coupled heat, moisture and stress field in freezing soil, Cold Reg. Sci. Tech., *Vol. 61*, pp. 417-429.

Sheng, D. (1994) Thermodynamics of freezing soils, theory and application, Doctoral Dissertation, 1994:141D, Luleå University of Technology.

Sheng, D., Knutsson, S., and Eigenbrod, D. (1992) Test and simulation of frost heave, 11th Nordic Geotechnical Meeting, Danish Geotechnical Society, Vol. 2, pp. 485-490.

Sheng, D., Axelsson, K., and Knutsson, S. (1993) Finite element analysis for convective heat diffusion with phase change, *Comp. Meth. Appl. Mech. Eng., Vol. 104*, pp. 19-30.

Sheng, D., Axelsson K., and Knutsson, S. (1994) Frost heave due to ice lens formation in freezing soils: 1. Theory and verification, *Nordic Hydrology, Vol. 26 (2)*, pp. 125-146.

Sheng, D., and Knutsson, S. (1993) Sensitivity analysis of frost heave – A theoretical study, Proc. 2nd Int. Symp. on Frost in Geotechnical Engineering (A. Phukan, ed.), Balkema, Rotterdam, pp. 3-16.

Address:
Department of Civil Engineering,
Luleå University of Technology,
S-971 87 Luleå,
Sweden.